Gallium-doped dual micro-nano titanium dental implants towards soft-tissue integration and bactericidal functions

Anjana Jayasree, María Natividad Gómez-Cerezo, Elise Verron, Sašo Ivanovski, Karan Gulati

Materials Today Advances 16 (2022) 100297

Contents lists available at ScienceDirect

Materials Today Advances

journal homepage: www.journals.elsevier.com/materials-today-advances/

Gallium-doped dual micro-nano titanium dental implants towards soft-tissue integration and bactericidal functions

Anjana Jayasree [a], María Natividad Gómez-Cerezo [b], Elise Verron [c], Sašo Ivanovski [a], Karan Gulati [a, *]

[a] The University of Queensland, School of Dentistry, Herston, QLD, 4006, Australia
[b] Departamento de Química en Ciencias Farmacéuticas, Facultad de Farmacia, Universidad Complutense de Madrid, Instituto de Investigación Sanitaria Hospital 12 de Octubre i+12, Plaza Ramón y Cajal s/n, 28040 Madrid, Spain
[c] Nantes Université, CNRS, CEISAM, UMR 6230, F-44000, Nantes, France

ARTICLE INFO

Article history:
Received 19 July 2022
Received in revised form
30 August 2022
Accepted 8 September 2022
Available online 1 October 2022

Keywords:
Titanium
Dental implants
Fibroblasts
Nanopores
Gallium
Antibacterial

ABSTRACT

Alongside osseointegration, effective soft-tissue integration (STI) is crucial to the long-term success of dental implants by preventing the ingress of oral pathogens. Nanoscale surface modification of titanium dental implants has shown promise in achieving enhanced bioactivity and antibacterial efficacy. We propose the fabrication of dual micro-nano anisotropic titania nanopores (TNPs) via electrochemical anodization of Ti, followed by incorporating gallium (Ga) towards enhanced antibacterial efficacy. Optimization of Ga chemical functionalization on TNPs was followed by in-depth surface topographical/chemical characterizations and *in vitro* Ga release. This study revealed that the surface chemistry, hydrophilicity, and topography of the TNPs were altered upon Ga-doping, resulting in the formation of Ga-containing nanoscale particulates firmly bound to TNPs. Further, gingival fibroblast bioactivity was favorably maintained on TNPs and Ga-releasing TNPs. Finally, a human oral salivary biofilm model confirmed the significant antibacterial efficacy of Ga-doped TNPs. Ga-doped dual micro-nano Ti dental implants are suitable as the next generation of bioactive and bactericidal dental implants.

1. Introduction

Dental implants have been widely applied in oral restoration and have demonstrated clinical success in replacing damaged or missing teeth [1]. A dental implant's stability primarily depends upon forming a bond between the surrounding bone tissue and the implant surface (osseointegration). Despite their high success rate, 5–10% of dental implants fail due to biomechanical overload, poor osseointegration, inflammation, or infection at the implant site [2,3]. Further, appropriate soft-tissue integration (STI) at the implant's transmucosal component is crucial for forming a soft-tissue seal that acts as a physical and physiological barrier preventing the ingress of oral pathogens into the underlying tissue [4].

Titanium (Ti) is an ideal material for dental implants due to its biocompatibility, superior mechanical properties and high corrosion resistance [5]. Several approaches have improved implant bioactivity by modifying the surface of Ti-based implants to alter surface topography and chemistry [6]. The ability to modulate cellular responses based on nanoscale roughness/features makes implant nano-engineering (1–100 nm) highly preferable over microscale modifications [1]. Among the various implant nano-engineering strategies like atomic layer deposition, lithography and electrochemical anodization (EA), anodization stands out due to its cost-effectiveness, scalability and ease of control over the nanostructure characteristics [1]. EA involves immersion of the Ti target/implant (anode) and a counter electrode (cathode, usually Ti or Pt) in an electrolyte containing fluoride ions and water and application of voltage/current using a DC power supply [1]. The chemical balance between the formation and dissolution of the oxide layer on the anodic surface leads to the self-ordering of various metal-oxide nanostructures.

Various titania (TiO_2) nanostructures like titania nanotubes (TNTs) and titania nanopores (TNPs) can be fabricated on the implant surface by varying EA voltage, current, electrolyte composition, and time [7]. More recently, TNPs (nanotubes with top nanoporous layer) synthesized via one-step anodization on micro-

* Corresponding author. School of Dentistry, University of Queensland, 288 Herston Road, Herston, QLD, 4006, Australia.
E-mail address: k.gulati@uq.edu.au (K. Gulati).

https://doi.org/10.1016/j.mtadv.2022.100297

rough Ti using reduced voltage/time and aged electrolyte (repeatedly utilized electrolyte) have emerged as a novel approach to modify implant surfaces [8,9]. TNPs fabricated by this method preserve the underlying implant micro-roughness and yield dual micro-nano scale topography that augment the functions of osteoblasts and fibroblasts [10,11]. Further, TNPs are aligned parallel to the underlying micro-machining, which mechanically stimulates cells towards parallel alignment [8].

While nanoscale implant surface modifications upregulate bone/soft-tissue integration, the nano-roughness also attracts bacteria. The promotion of bacterial adhesion or biofilm formation, especially in compromised conditions such as diabetes and smoking [3], can lead to peri-implantitis resulting in complete implant failure [12,13]. Conventional approaches to address implant-associated infections include systemic administration of antibiotics and surgical debridement based on severity [14,15]. Systemic antibiotic therapy may lead to systemic toxicity, development of antimicrobial-resistant strains, and poor penetration into the bacterial biofilms, while surgical debridement can further delay soft-tissue healing [16,17]. This has shifted the focus of implant therapy research to local drug release from the implant surface, utilizing modifications such as anodized nanotubes [1]. TNTs have been widely explored for the loading and local delivery of proteins, growth factors or antibiotics in a tailored fashion aimed at customizable local therapy, as previously reviewed [1,18].

Incorporation of unconventional antimicrobial agents such as metallic ions and nanoparticles like silver (Ag), zinc (Zn), copper (Cu), magnesium (Mg), hafnium (Hf) and gallium (Ga) have been utilized to achieve maximized local therapy without excessive toxicity [19–22]. The bioactivity of Ga^{3+} towards bone pathologies [23–25] and its broad spectrum antibacterial efficacy have led scientists to incorporate these ions in various biomaterials like bioglass [26], bio-ceramics [27], injectable apatitic cement [28] and 3D printed Ti surfaces [21]. Ga ions have been shown to replace iron (Fe) from the Fe-dependent redox reactions during DNA synthesis in bacteria, resulting in cell death in *Escherichia coli (E. coli), Staphylococcus aureus (S. aureus),* and even in drug-resistant strains like Methicillin-Resistant *S. aureus* (MRSA) [29]. Additionally, Ga enhances osteoblast growth, inhibits bone resorption, promotes collagen synthesis, and improves bone tissue formation [25,30,31]. These characteristics make Ga an appropriate therapeutic agent for dental implant modifications to enhance osseointegration and achieve increasing its antibacterial efficacy. Recent approaches to Ga-modified titanium nanostructures include TNTs [32], titanium nanopillars [21], TNTs coated with poly-DL-lactic acid (PLLA) [33] and polydopamine-functionalized $SrTiO_3$ nanotubes [34]. While these studies demonstrate the successful incorporation of Ga ions in Ti nanostructures, they are limited to orthopaedic implant applications (mainly osseointegration). Further, the antibacterial studies are limited to single bacterial species like *E. coli, S. aureus* and *Pseudomonas aeruginosa (P. aeruginosa)*, which does not represent the clinical scenario. Ensuring the long-term stability and success of dental implants is more challenging than orthopaedic implants, with the need for appropriate STI in addition to osseointegration. Further, the oral cavity is comprised of a wide variety of microorganisms residing in a protective biofilm that increases the risk of infection at the implant site. Despite its influence in enhancing osseointegration and antibacterial efficacy, studies evaluating the effect of Ga on STI are lacking. In the current study, we assessed the bioactivity of human gingival fibroblasts cultured at the surface of Ga-doped dual micro-nano Ti dental implants toward STI. We evaluated the bactericidal action of the Ga-doped implants in an oral salivary polymicrobial biofilm model.

Development of Ga-doped nanoporous Ti dental implants included the following specific aims (Fig. 1):

a. To optimize the Ga functionalization of micro-rough nanoporous implants and perform in-depth surface topography and chemistry characterizations.
b. To evaluate the effect of Ga-doped surfaces on human gingival fibroblast activity by observing cell viability, proliferation, and alignment.
c. To investigate the antibacterial efficacy of the Ga-doped surfaces on oral salivary biofilm by observing its attachment, thickness, and metabolic activity.

2. Materials and methods

2.1. Fabrication of TNPs by electrochemical anodization

Ti flat foils (99.5% purity, 0.25 mm thick) were purchased from Alfa Aesar (UK). The components of the electrolyte, including ammonium fluoride (NH_4F, ≥ 99%) and ethylene glycol (≥99%) (EG), were purchased from Sigma-Aldrich (Australia). Before anodization, the Ti foils were mechanically prepared using various grades of sandpaper to create a micro-roughened surface **(Micro-Ti)** [10,35]. These Micro-Ti surfaces were then rinsed with ethanol and cut into squares of 1 cm^2. These foils were cleaned thoroughly by ethanol sonication twice and air-dried before anodization. Ethylene glycol electrolyte comprised of 1% water (v/v) and 0.3% NH_4F (w/v) was prepared and further pre-conditioned (aged) by anodizing a non-target Ti surface as described previously [36]. In a custom-designed electrode system, Micro-Ti as anode and non-target Ti as cathode were immeresed in the electrolyte. Keysight E36106A DC power supply was used to supply constant voltage to the electrochemical cell. Single-step anodization was carried out at 60 V for 10min to obtain nanopores **(TNPs)**, which were finally cleaned with deionized water and air-dried before use [8].

2.2. Preparation of Ga-doped Ti surfaces

The incorporation of Ga was carried out on both micro and TNP surface. Ga was incorporated into the substrates by soaking them in a 1 mg/mL aqueous solution of $Ga(NO_3)_3 4H_2O$. Then, the pH of the solution was adjusted in the 9.2–9.8 range using a concentrated NaOH solution followed by stirring at room temperature for 6 h and air drying for 24 h. The Ga-incorporated Micro-Ti and TNP surfaces (**Ti–Ga and TNP-Ga,** respectively) were finally rinsed with deionized water and air-dried before use.

2.3. Characterization of surface topography of Ga-doped Ti

The surface topography of the Ga-doped Ti substrates was visualized using a field-emission scanning electron microscope (FESEM, JEOL-JSM 7001F). The substrates were mounted on an SEM holder using double-sided carbon tape, followed by plasma cleaning before imaging.

The surface roughness of the substrates was characterized using Bruker ICON XR atomic force microscope (AFM). Three random areas (1 μm × 1 μm) on each sample were analyzed and their root mean square (Ra) and roughness average (Ra) was calculated.

2.4. Surface chemistry characterizations of the Ga-doped Ti

X-ray Photoelectron Spectrometer (XPS) data sets of the substrates were measured using a Kratos Axis ULTRA X-ray photoelectron spectrometer incorporating a 165 mm hemispherical electron energy analyzer. Survey (wide) scans were carried out over the 1200–0 eV binding energy range with 1.0 eV steps and a dwell time of 100 ms on three substrates per group to characterize their

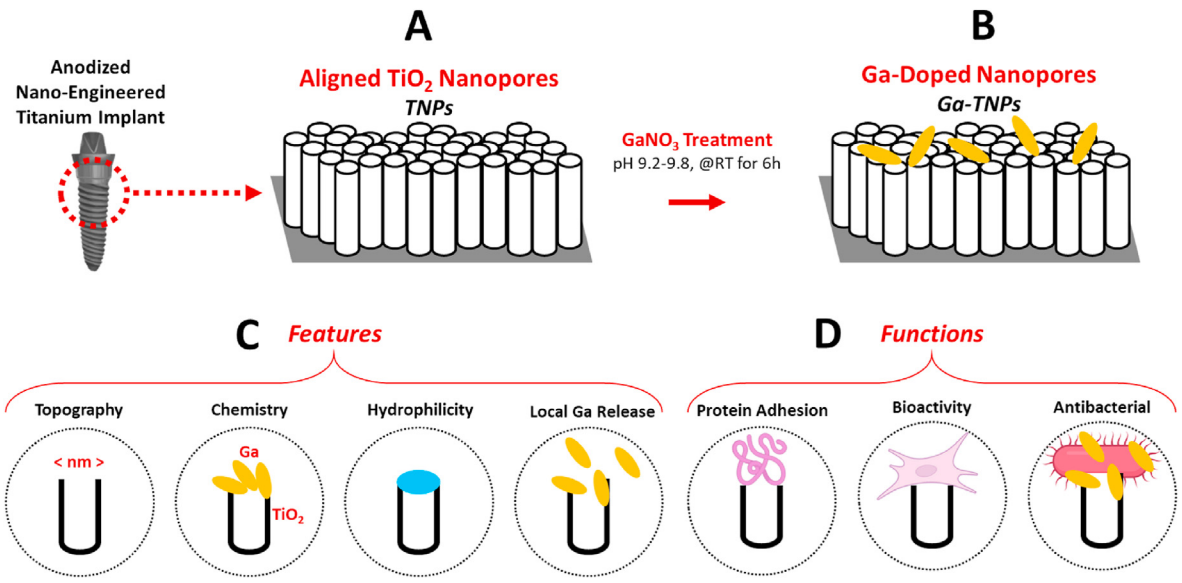

Fig. 1. Ga-doped therapeutic dental implants. Schematic representation: (A) anodization of Ti implants to fabricate nanopores; (B) doping of Ga on nano-engineered Ti implants; (C) characteristics of the modified implant; and (D) bioactivity and antibacterial functions.

element compositions (atom %). Furthermore, narrow high-resolution scans were run within 20 eV with 0.05 eV steps and a 250 ms dwell time on various Ti surfaces, which focused the Ga 2p, Ti 2p, and O 1s narrow-spectrum on each sample. Peak fitting and analysis of composition were carried out in CasaXPS version 2.3.14, using a Shirley baseline model, mixed Gaussian/Lorentzian 70:30 line shapes, and the Kratos Relative Sensitivity Factor (RSF) library. Data sets were charge-referenced to the C 1s hydrocarbon peak at 284.8 eV BE.

For X-ray diffractometer (XRD) characterization, substrates were analyzed on a Bruker D8 Advance X-ray diffractometer equipped with a Cu anode operated at 40 kV and 40 mA, a Lynxeye XE energy discriminating 2D array detector to minimize fluorescent backgrounds, and an automated knife edge to allow simultaneous measurements at low and high angles. Diffraction patterns were recorded by continuous scans at 10–80° (2θ) with a step size of 0.02° at a scan rate of 2° per min. The resulting patterns were imported into Diffrac EVA version 5.1, where phases were identified using the PDF-4 2020 ICDD database.

Water contact angles (WCA) on the substrates were evaluated using Dataphysics OCA 15 EC, a contact angle goniometer. 2 μL of water was placed on each substrate, and a photograph was captured after 3s using a high-resolution camera, followed by a calculation of contact angle using SCA 20 software (ellipse fitting method).

2.5. In vitro Ga release

Ga released from the Ti/TNP surfaces were analyzed by immersing the substrates in 5 ml PBS with gentle shaking at 37 °C. A definite volume of release buffer was withdrawn at specific intervals and replaced with fresh PBS. The amount of Ga ions released was quantified using inductively coupled plasma mass spectrometry (ICP-MS).

2.6. Evaluation of protein adhesion

Protein adhesion on various substrates was evaluated using a BCA protein assay kit (Novagen, Australia) described previously [36]. The substrates were immersed in fetal bovine serum (FBS; Gibco®, Australia) for 4 h at 37 °C with gentle shaking. The substrates were then rinsed with PBS to remove unbound protein, followed by repeated flushing with 2% (w/v) SDS (Sigma-Aldrich, Australia) to extract the adhered protein. The amount of protein was quantified using the BCA kit per the manufacturer's protocol, and optical density was measured at 562 nm using a TECAN Infinite M200 PRO spectrophotometer.

2.7. Human gingival fibroblast (hGF) cell culture

Primary hGF cells were isolated from excised gingival tissue from healthy patients with consent and institutional ethics approval (The University of Queensland; Human ethics approval number 2019000134) using previously reported methodology [37]. Briefly, the isolated tissue was placed in Dulbecco's modified eagle's medium-high glucose (DMEM; Life Technologies, Australia) containing 10% (v/v) fetal bovine serum (FBS; Gibco®, Australia) and 4% (v/v) penicillin-streptomycin-glutamine (PenStrep; Gibco®, Australia) at 37 °C with 5% CO_2. The fibroblasts growing out of the explants were subcultured for further use. The cells of passages 4–6 were used for experiments.

Ti substrates were sterilized by rinsing with 70% (v/v) ethanol followed by UV irradiation for 30min/per side. Each substrate was seeded with 3.5×10^3 cells and incubated at 37 °C with 5% CO_2 for 2 h to facilitate attachment of cells onto the substrate, followed by the addition of DMEM supplemented with 10% (v/v) FBS and 1% (v/v) PenStrep.

2.8. Live/dead assay of hGF on Ti substrates

To evaluate the potential toxicity of Ga release on hGFs, live/dead staining was carried out on days 1, 3, and 7. The substrates were rinsed with PBS, followed by incubation in a staining solution comprised of 5 μg/ml fluorescein diacetate (FDA, Sigma-Aldrich, Australia) and 2 μg/ml of propidium iodide (PI, Sigma-Aldrich, Australia), as described previously [8]. The stained substrates were then visualized using Leica TCS SP5 scanning laser confocal microscope (Leica Microsystems, Mannheim, Germany) at excitation/emission (Ex/Em) 488/526 nm for FDA and Ex/Em 493/636 nm for PI.

2.9. Evaluation of cellular attachment and morphology

The hGF-seeded substrates were taken out at specific time points (1 h, 6 h, days 1, 3, and 7) and fixed with 4% (w/v) paraformaldehyde (PFA) for 20 min. The substrates were then immersed in a staining solution comprised of 5 μg/mL of 4,6-diamino-2-phenylindole (DAPI; Life Technologies, USA) and 0.8 U/mL Alexa fluor 568 phalloidin (Life Technologies, USA). The morphology and alignment of the cells on the substrate were captured using Leica TCS SP5 scanning laser confocal microscope (Leica Microsystems, Germany), and quantification of nucleus aspect ratio and actin alignment was performed using *ImageJ* software.

To further visualize the cellular morphology, the PFA fixed substrates were dehydrated in a series of graded ethanol concentrations (50, 70, 90, 95, and 100%), air-dried, and mounted on SEM stubs using conductive double-sided carbon tapes. The substrates were then coated with a 5 nm thick layer of platinum, plasma cleaned, and imaged using JEOL-JSM 7001F SEM.

2.10. Cell proliferation

To evaluate the cellular proliferation on the substrates, the amount of DNA was quantified at specific time intervals (days 1, 3, and 7) using a Picogreen dsDNA quantification assay kit (Invitrogen, Australia). The substrates were removed from the media at specific time points and were treated with 5 mg/mL of proteinase-K (Invitrogen, Australia) solution at 56 °C for 8 h [8]. The amount of DNA in the cell lysate was evaluated following the manufacturer's protocol, and the fluorescence was measured at Ex/Em 480/520 nm using TECAN InfiniteM200PRO.

2.11. Development of salivary biofilm on various Ti substrates

Unstimulated saliva was collected from healthy individuals with good gingival health with consent and institutional ethics approval (The University of Queensland, institutional human ethics committee, approval number: 2019001113) by established protocols [8]. The saliva was mixed with an equal volume of 70% (v/v) glycerol stock solution and stored at −80 °C for further use.

To prepare the inoculum, 1 ml of the glycerol stock was mixed with 10 ml of brain heart infusion media (BHI, Merck, Australia) and cultured under anaerobic conditions at 37 °C with gentle shaking overnight.

Ti foils were rinsed with 70% (v/v) ethanol followed by exposure to UV for 30min/side before the experiment. The substrates were placed in fresh 24 well plates and 1 ml of BHI media containing 5% of defibrinated sheep's blood and 1×10^6 CFU of overnight inoculum was added and cultured under anaerobic conditions at 37 °C with gentle shaking.

2.12. Live/dead staining of biofilm

To evaluate the antibacterial efficacy, the substrates were stained using a LIVE/DEAD™ BacLight™ bacterial viability kit (Life Technologies, Australia) per the manufacturer's protocol. The substrates were retrieved at specific time points (days 1, 3, and 7), washed with PBS to remove unattached biofilm, and finally stained with SYTO™ 9 and propidium iodide (PI) (3 μL of each dye/mL of PBS) for 30min. The stained substrates were rinsed with PBS and visualized using a confocal microscope (Leica TCS SP5).

2.13. Quantification of biofilm

The substrates were extracted on days 1, 3, and 7 and washed twice with PBS to remove unattached biofilm. A crystal violet assay was performed to quantify the total biofilm formed as described previously [8]. Briefly, the substrates were stained with 0.1% crystal violet (Sigma-Aldrich, Australia) for 15min, followed by treatment of 10% (v/v) acetic acid for 30min to solubilize the bound dye. The absorbance was measured at 570 nm using TECAN InfiniteM200PRO.

2.14. Evaluation of metabolic activity of the biofilm

The metabolic activity of the biofilm formed on the substrates was evaluated using tetrazolium salt, 2,3-bis (2-methoxy-4-nitro-5-sulfophenyl)-5-[(phenylamino) carbonyl]-2H-tetrazolium hydroxide (XTT, Sigma-Aldrich, Australia). The substrates were retrieved at specific time points (days 1, 3, and 7) and washed twice with PBS to remove any unbound biofilm. 1 ml of working XTT solution (0.4 mM Menadione + PBS + XTT in the ratio 79:20:1(v/v/v)) was added to the substrates and incubated in the dark at 37 °C for 4 h. The absorbance was measured at 492 nm using TECAN InfiniteM200PRO.

2.15. Characterization of biofilm morphology

At specific time intervals, the substrates were extracted from the media and treated with 4% PFA, followed by gradient ethanol treatment (50, 70, 90, 95, and 100%) for fixing and dehydrating the biofilm. The substrates were then mounted on SEM stubs using conductive carbon tapes, coated with a 5 nm thick layer of platinum, plasma cleaned, and imaged using JEOL-JSM 7001F SEM.

2.16. Statistical analysis

All the experiments were carried out in triplicates and the results are represented as mean ± standard deviation. Two-way analysis of variance (ANOVA) and Tukey's multiple comparison test was carried out using GraphPad Prism 7 software to evaluate the statistical significance, and p values < 0.05 were considered statistically significant.

3. Results and discussion

3.1. Ga-doped nanopores: surface topography characterization

Unidirectional microgrooves were observed on the mechanically prepared Ti foils (Micro-Ti, Fig. 2a), which mimic the micromachining lines usually found on the surface of dental implants. Previous reports indicate that single-step anodization of microrough Ti yields TNPs, which conserve the underlying microscale roughness/features, thereby producing a dual micro-nano structured surface [10,38]. We have previously shown that TNPs have superior mechanical stability compared to conventional nanotubes [36]. Further, TNPs can be fabricated on clinically relevant complex implant topographies like Ti screws and enhance osseointegration [8,35].

Electrochemical anodization of Micro-Ti at 60 V for 10 min using an aged electrolyte yielded TNPs of 57 ± 4 nm that aligned parallel along the underlying microgrooves (Fig. 2c). TNPs fabricated at 60 V-10min have previously been demonstrated to enhance the expression of osteogenic markers like ALP and aid in osseointegration [8]. These nanopores have nanotubular structures underneath (nanotubes with a top nanoporous layer) (Figure S1, Supplementary Information). Further, EDS analysis of TNPs confirms the presence of F on the surface, which is lacking on Micro-Ti. It is noteworthy that F^- gets incorporated within the anodic film during anodization, and its effective removal is difficult to achieve (Figure S2, Supplementary Information).

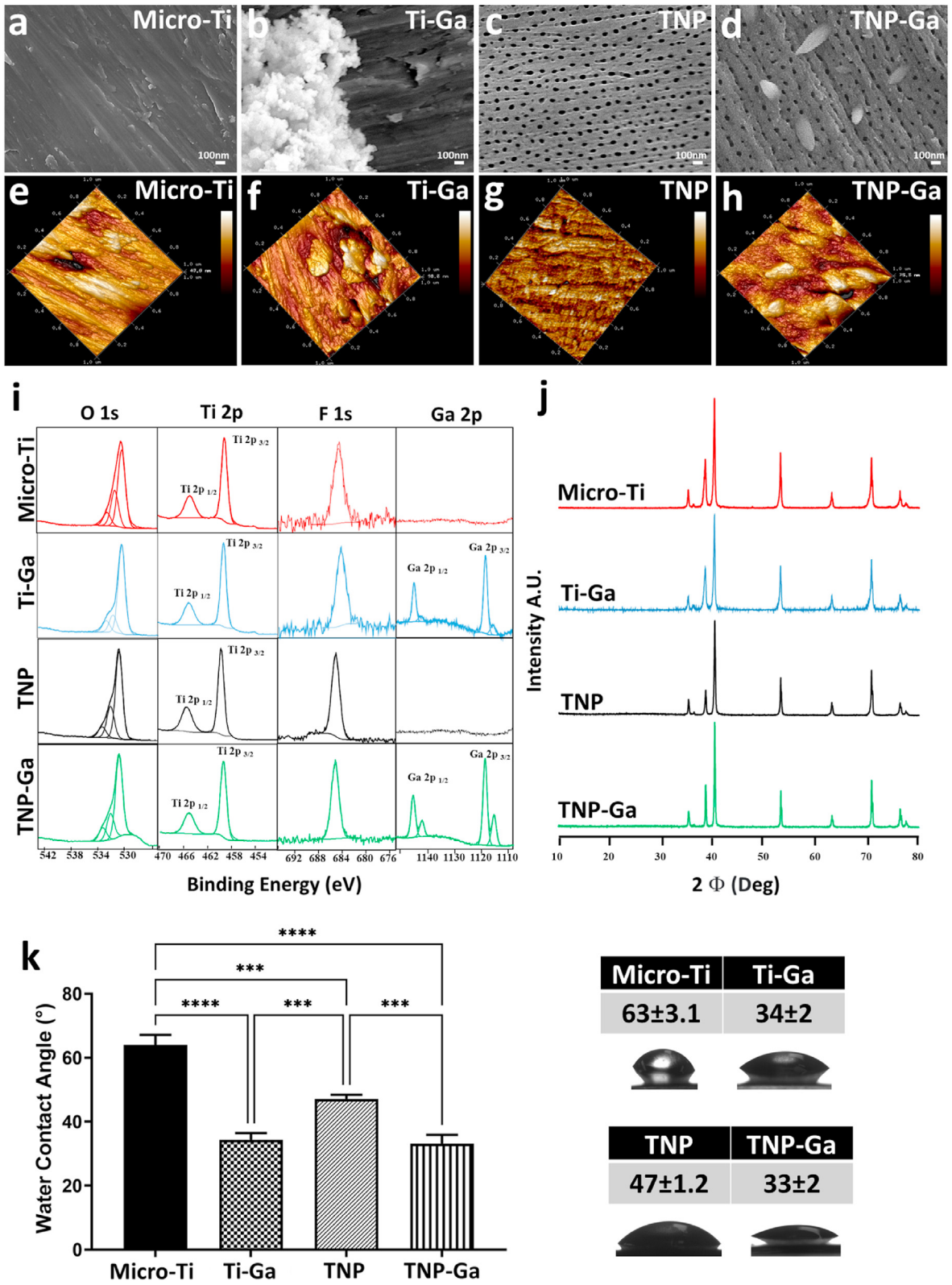

Fig. 2. Surface topography and chemistry characterizations of various Ti substrates. (a–d) Top-view SEM images; (e–h) AFM micrographs; (i) XPS wide scan surveys showing the incorporation of Ga on Ti–Ga and TNP-Ga surfaces; (j) XRD spectra showing Ti and TiO_2 phase present within all the groups indicating that anodization and Ga doping did not alter the phase of the underlying Ti; and (k) surface wettability of Ti surfaces. Anodization and the incorporation of Ga significantly increased the hydrophilicity of the surface. **Micro-Ti**: mechanically prepared Ti foils; **Ti–Ga**: Micro-Ti foils doped with Ga; **TNP**: titania nanopores fabricated at 60 V, 10min; **TNP-Ga**: TNP doped with Ga.*: Significant difference between the groups. (**-p<0.01, ***-p<0.001).

Optimization of Ga doping on TNPs was performed by immersion of the substrates in $Ga(NO_3)_3 4H_2O$ of various concentrations, pH and time of incubation. Initially, TNPs were immersed in $Ga(NO_3)_3 4H_2O$ solution of concentration 1 mg/mL and 3 mg/mL in acidic (pH 3) and alkaline (pH 9) conditions for 24 h, followed by air drying. At acidic conditions, no visible differences were observed on the TNP surfaces, however, Ga deposits were observed under alkaline conditions (Figure S3, Supplementary Information). Treatment of TNPs with 1 mg/ml at pH 9 was selected for further experiments as minor delamination of TNPs was observed at 3 mg/mL. Ga doping at various time points (1 h, 3 h and 6 h) demonstrated that a uniform deposition of rice-like structures was obtained on TNPs after 6 h of treatment (Figure S4, Supplementary Information).

Micro-Ti and TNPs were functionalized with Ga by immersion in $Ga(NO_3)_3 4H_2O$ for 6 h in alkaline condition to obtain Ti—Ga and TNP-Ga, respectively. Interestingly nanoscale rice-like depositions (referred to as nano-rice) scattered throughout the surface were observed on TNP-Ga (Fig. 2d), while agglomerations were found on Ti—Ga (Fig. 2b). EDS analysis of Ti—Ga and TNP-Ga shows Ga presence, confirming that Ga incorporation was successful. (Figure S2, Supplementary Information). Previous reports indicate that Ga ions in the solution can interact with the hydroxide ions in the water at alkaline pH to form impulsive nuclei, which gradually grow into nanostructures and get deposited onto the Ti surfaces [39,40]. As reported earlier, alkaline conditions favor the formation of Ga_2O_3 and the deposition of rice-like structures [39]. The formation of nuclei leading to the deposition of Ga on the surfaces is highly spontaneous and depends on the type of precursors and surface properties of the substrate [39]. While the precursors remain constant, the surface topography and chemistry of Micro-Ti and TNPs are very different, which results in the difference in Ga depositions on these surfaces [8].

Next, the surface topography and roughness were evaluated using AFM (Fig. 2e—h). Micro-Ti surfaces had a crest and trough-like morphology with the lowest surface roughness. Post anodization, the substrates demonstrated a nanotopography that preserved the underlying micro-grooves generating a micro-nano topography [8]. The age of the electrolyte (conditioning of electrolyte with multiple cycles of anodization using non-target Ti) used for anodization plays a significant role in conserving the underlying topography by regulating chemical balance (increased pH and TiF_6^{2-} ions; and reduced conductivity and free F ions) [38]. The deposition of Ga nano-rice and clusters on TNP-Ga and Ti—Ga further increased the surface roughness of the substrates, following the trend: Micro-Ti < TNP < Ti—Ga = TNP-Ga (Figure S5, Supplementary Information).

3.2. Ga-doped nanopores: surface chemistry characterization

To thoroughly characterize the surface chemistry of the various substrates, the elemental composition of Ti, O, F, and Ga was evaluated using a wide scan XPS survey, and the successful incorporation of Ga into Micro-Ti and TNPs was demonstrated (Table S1, Supplementary Information). Compared to Ti—Ga, the elemental composition of Ga on TNP-Ga was found to be significantly higher. High-resolution narrow scans on Ga 2p, Ti 2p, O1s, and F1s were conducted to explore surface chemistry alterations (Fig. 2i). Similar XPS spectra with O1s (531eV) and Ti2p (458eV) peaks were observed for all substrates indicating the presence of TiO_2 [41]. Ti—Ga and TNP-Ga show two significant Ga2p peaks at 1145.5 and 1118.6 eV, respectively, which refers to the Ga2p1/2 and Ga2p3/2 signals that attribute to the native oxide form of Ga (Ga^{3+}) as Ga_2O_3 [34,42]. TNP-Ga shows an additional peak at 531.5 eV (absent in Ti—Ga) in the O1s region, which corresponds to the Ga—O bond [43], indicating the possibility that the form of Ga deposited on the TNPs might be oxide in nature.

Further, the crystalline structure of the modified surfaces was studied using XRD (Fig. 2j). Micro-Ti and TNP surfaces showed peaks (2θ degree) corresponding to the Ti (ICDD 01-089-5009) and TiO_2 (ICDD 03-065-6429) phase with similar intensity, indicating that anodization did not alter the phase of the Ti. As expected, the Ga-doping of Micro-Ti and TNP did not change the crystalline phase of the underlying Ti.

The wettability of an implant surface is a critical parameter that influences the adhesion of blood/plasma proteins, the interaction of cells, and bacterial adhesion [44,45]. While hydrophilic surfaces have been shown to augment the proliferation and attachment of osteoblasts and fibroblasts [46,47], they have been reported to significantly reduce bacterial adhesion [48] as bacteria interact with surfaces using hydrophobic interactions. TNPs have significantly higher hydrophilicity than Micro-Ti, indicating that anodization can enhance surface wettability, which agrees with previous reports [8]. The incorporation of Ga on the surfaces further increased the hydrophilicity, following the trend: Micro-Ti < TNP < Ti—Ga = TNP-Ga (Fig. 2k).

Surface chemistry and surface topography play major roles in regulating the wettability of a surface. Wenzel et al. established that surface roughness and WCA are inversely proportional and that when the roughness of a surface increases, its wettability also increases [49]. AFM analysis in Figure S5 (Supplementary information) demonstrates increased surface roughness of TNPs and Ga-loaded surfaces, with a similar pattern also observed in wettability. Nanopore porosity can also increase surface wettability, as pores can trap water and create a capillary effect that can reduce the water contact angle (increase hydrophilicity) [50]. Previously, the incorporation of Ga on TNTs on 3D printed surfaces showed no significant effect on the hydrophilicity of the substrates [32]; however, we observed a significant improvement in the hydrophilicity of both Micro-Ti and TNP upon Ga incorporation.

3.3. Release of Ga from nanopores in vitro

The '*race to invade*' the dental implant surface between the host cells and the microbes present in the oral microenvironment begin within minutes of implantation. The outcome of this 'race' plays a significant role in determining the success of an implant [4]. The initial 48 h is critical, within which bacteria can adhere to the implant surface and begin the formation of pellicles that can lead to biofilm formation. We observed an initial burst release of Ga ions at 6 h with 2 μg of Ga released within the first 10 min from both Ti—Ga and TNP-Ga surfaces which can aid in preventing the early adhesion of microorganisms (Fig. 3a). Though the Ga release from Ti—Ga peaked at day 1 (8 μg) and dropped to <1 μg by day 7, TNP-Ga showed a more sustained release with a release of 2 μg on day 10. While drop-casting of Ga on TNTs showed a total release of 90% within day 5 [32], we observed that doping of Ga on TNPs could prolong the release to 10 days. Despite the prolonged release of Ga from polydopamine-coated TNTs (15 days), the amount of Ga released was very low (ppm range) [34]. In the current study, higher release (μg range) was observed, indicating the superior therapeutic efficacy of our system that can be utilized to target polymicrobial infections in a clinical scenario.

3.4. Evaluation of protein adhesion capacity

Upon implantation, the surface of implants primarily encounters blood and serum proteins. This interaction is crucial in activating a cascade of events that leads to tissue integration and implant stability. Surface chemistry, wettability and surface area of

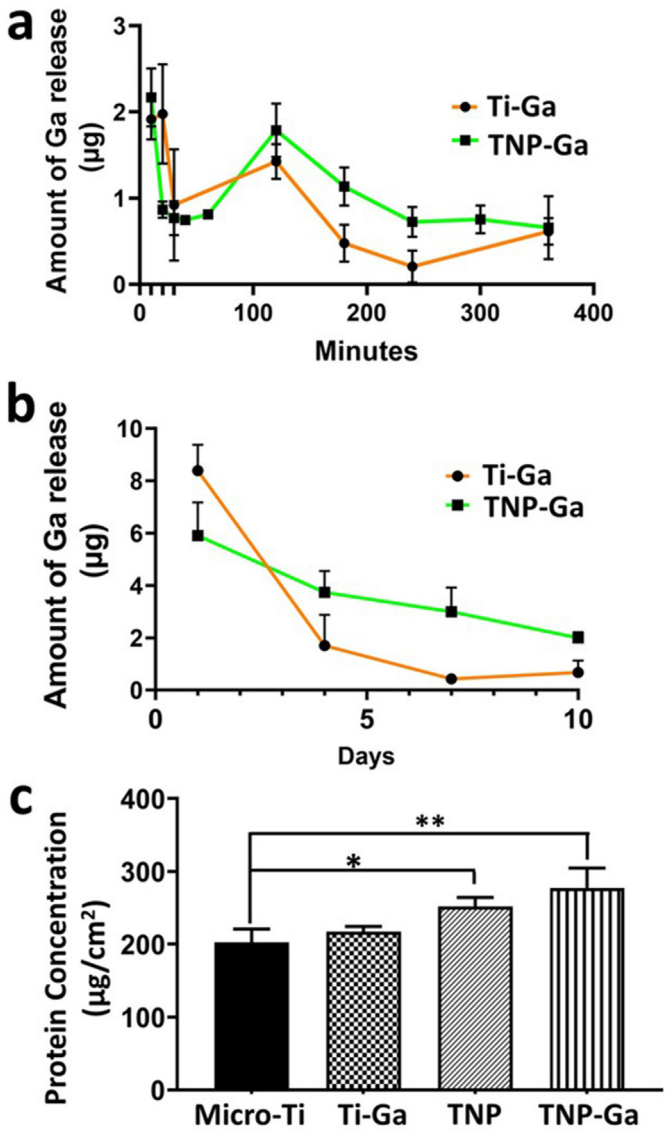

Fig. 3. Ga ion release kinetics and protein adhesion. (a) Initial burst release (IBR) within 6 h from Ga-doped Ti surfaces; and (b) prolonged release of Ga from the doped substrates. (c) Protein adhesion on doped and undoped Ti surfaces showed that Ga doping did not have a significant influence on protein adhesion. *: Significant difference between the groups. (*-p<0.05, **-p<0.01).

the implant play a significant role in regulating these interactions and nano-topographies have been shown to augment protein adhesion [51]. In our study, anodization increased the protein adhesion on the surface compared to Micro-Ti. At the same time, doping of Ga did not show any significant difference, following the trend: Micro-Ti < Ti–Ga < TNP = TNP-Ga (Fig. 3c). An increase in surface roughness and wettability augments protein adhesion, comparable to the enhanced adhesion observed in the case of TNPs and TNP-Ga. Our results were congruent with previous studies where Ga-loaded nanotubes were coated with polydopamine [34]. Despite the increase in surface roughness and wettability of Ti–Ga and TNP-Ga, they showed no significant difference in protein adsorption compared to their undoped counterparts. This might be caused due to the electrostatic interactions between the Ga ions and the proteins [52].

3.5. Stability and cytotoxicity of Ga-doped surfaces

An essential criterion of implant surface modification is mechanical stability, as any delamination and release of nanoscale debris can cause local cytotoxicity [53]. TNPs have superior mechanical properties as compared to conventional nanotubes, as established elsewhere [36]. TNPs outperform conventional nanotubes and physically/chemically enhanced TNTs in terms of mechanical robustness. To determine if the Ga nanorice will detach from the TNP-Ga surfaces, we immersed the substrates in DMEM containing 10% (v/v) FBS and 4% (v/v) PenStrep at 37 °C with gentle shaking (100 rpm) for 1, 3 and 7 days, and the top-view SEM images are presented in Fig. 4a–c. Although the nanorice was observed on the TNPs at all three time points, the frequency/number was lower as the days progressed, indicating that the Ga deposits undergo gradual dissolution within the media, similar to previous observations on TNT surfaces [32]. While the complete dissolution of Ga was observed from TNTs within 5 d, we could observe the presence of nanorice even after 7 d. Next, we performed sonication of TNP-Ga surfaces in PBS for 2 min and 5 min to check if the sonication process would remove the Ga depositions. Sonication of TNP-Ga for 2 min and 5 min showed no changes in the surface morphology, indicating that the nanorice adhered firmly to the TNPs (Fig. 4d–f).

Despite their potential to elicit antibacterial efficacy, localized delivery of metallic ions and nanoparticles has raised concerns about local and systemic toxicity [54]. For dental implants, the evaluation of cytotoxicity is crucial as the implants are in constant contact with the oral cavity and the metallic ions released or leached from these surfaces are highly likely to be ingested and finally absorbed by the digestive tract. Milheiro et al. observed that at 100 ppm concentration, gallium nitrate showed toxicity toward mouse fibroblasts [55]. Fe^{3+} ions play a significant role in cellular metabolism by forming ligands with various molecules like transferrin [56]. Ga^{3+} ions can form coordination bonds like Fe^{3+} ions and thereby easily replace Fe^{3+} and chelate with other proteins and ligands, eventually interfering with cellular metabolism [56]. Excessive Ga^{3+} uptake by cells can even interfere with DNA replication and lead to cell apoptosis. In the current study, we observed that even when showing the highest drug release (1 d), no cytotoxicity effects were observed in gingival fibroblasts on both Ti–Ga and TNP-Ga surfaces (Fig. 4g). Irrespective of the Ga ion release, the cells were observed to be well spread. The increase in cellular density on the substrates on days 3 and 7 indicated that Ga ions did not inhibit cellular proliferation.

3.6. Investigating soft-tissue integration ability of TNP-Ga implants

3.6.1. The proliferation of gingival fibroblasts

Picogreen assay was used to evaluate the effect of nano-topography and Ga content on the proliferation of human gingival fibroblasts. The surface roughness and wettability of the nanopores have been shown to enhance fibroblast proliferation [7]. A similar result was observed, with TNPs showing the highest proliferation rate than other groups on days 3 and 7 (Fig. 5b). The uptake of Ga ions by tumor cells like HeLa has shown to hinder the Fe ion uptake leading to disruption of cell replication and reduction in cellular proliferation [56]. Meanwhile, Ga ions neither inhibited nor promoted the proliferation of osteoblasts [25,26]. In the current study, the presence of Ga did not show any significant effect on cell proliferation. Compared to the tumor cells, fibroblasts have a low number of Fe receptors (e.g., transferrin) that might result in lower uptake of Ga, thus minimizing the effect of Ga on cell metabolism.

3.6.2. Fibroblast adhesion and alignment

Soft-tissue integration (STI) at the transmucosal region of a

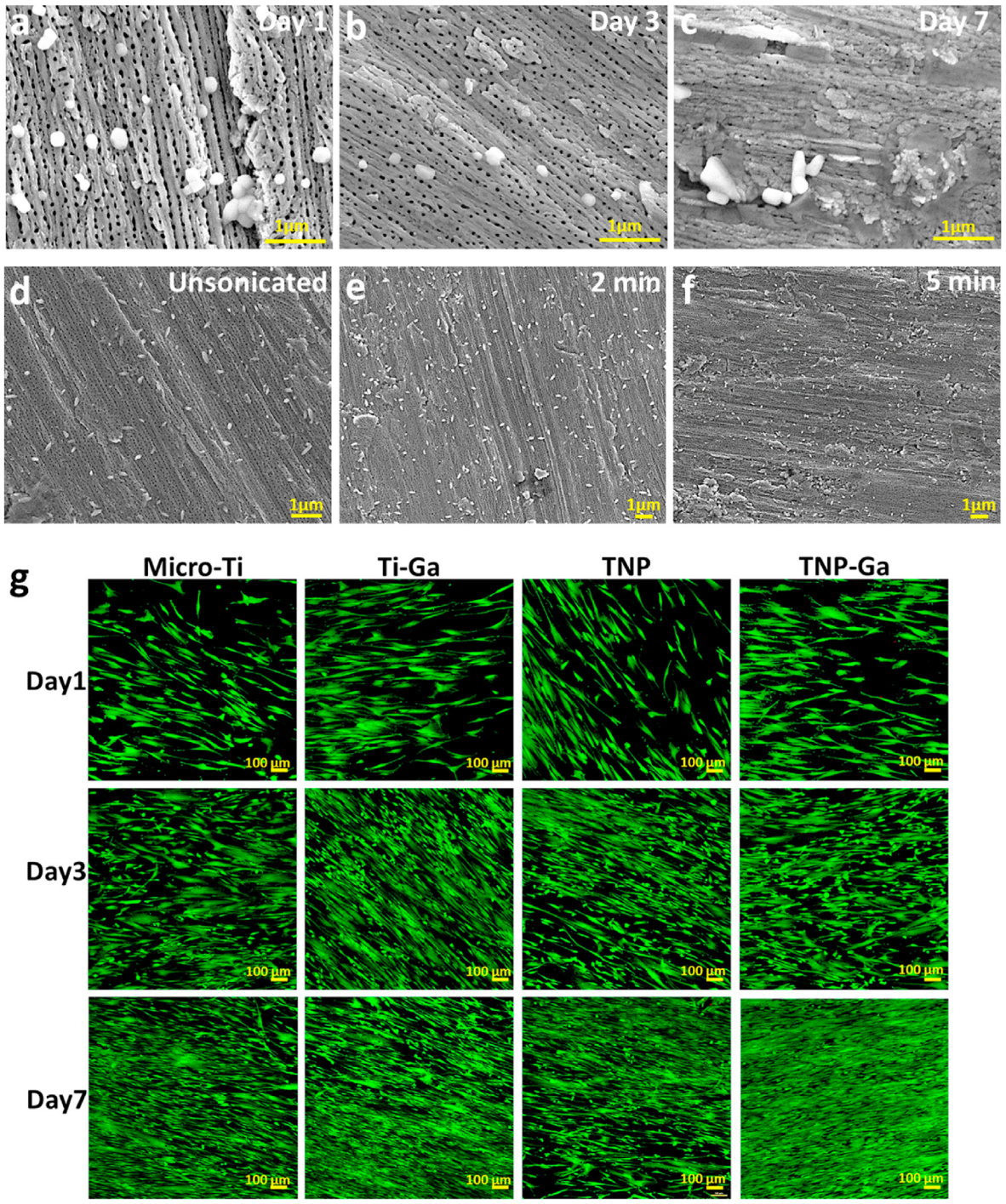

Fig. 4. Stability and cytotoxicity analysis of Ga-doped Ti. Top-view SEM images showing: (a–c) Stability of Ga doping observed in cell culture media on days 1, 3 and 7; and (d–f) effect of sonication on Ga doping on TNP. (g) Live/dead staining of hGFs on various Ti surfaces on days 1, 3, and 7 were visualized by confocal microscopy. (Green stain: live cells, red stains: dead cells). (For interpretation of the references to colour in this figure legend, the reader is referred to the Web version of this article.)

dental implant is crucial to facilitate the formation of a tight epithelium cuff and strong connective tissue seal and the longevity of the implant [5]. The integration and maturation of gingival fibroblasts onto the implant surface lasts 4–12 weeks and is crucial for the secretion of collagen and other extracellular matrix components [4]. Fibroblasts are highly sensitive toward surface topography and have demonstrated directional attachment on grooved micro and nano surfaces [7]. While the effect of TNPs and their topography on fibroblast activity and STI have been studied in detail, an investigation into the impact of Ga ions on STI is lacking. In the current study, we evaluated the effect of Ga and topography of Ti on the attachment and alignment of gingival fibroblast at early time points of 1 h, 6 h, and 24 h, and later time points of days 3 and 7. The hGFs were observed to align along the underlying microgrooves on all the substrates from the early time point of 6 h (Fig. 5a). The cells appeared to have a circular shape at 1 h, gradually spreading along the underlying topography to attain spindle-like morphology by 6 h. As established previously, dual micro-nano

TNPs augment cytoskeletal filapodial extensions of fibroblasts and modulate mechanotransduction [7] that stimulates the cells to align parallelly along the underlying nanopores. The alignment of actin filaments and the aspect ratio of the cellular nuclei were further quantified (Figures S6a and b, Supplementary Information). While no significant difference was observed between the Ga-doped and undoped counterparts, TNPs showed a slightly higher actin alignment early point of 6 h, indicating that the dual micro-nano topography attributed to the higher alignment of the cells. A similar pattern was observed for the nuclear aspect ratio. While Ga-doping did not influence the fibroblast attachment and alignment, bare TNPs showed an increased cell spreading.

High magnification SEM imaging was carried out at 6 h and 24 h, and day 3 to further observe the close interaction between TNPs, Ga-doping and hGFs (Fig. 5c). Nanoscale projections from the cellular body called nanopodia can interact with surface topographies smaller than 15 nm and play a significant role in attachment and cellular alignment [57]. Several nanopodia-like structures could be observed extending from the cell body externally, indicating cell-surface communication. The Ga deposits were observed to have no toxic/inhibitory effects on cell spreading, as filapodial extensions could be observed over the Ga nanorice structures.

3.7. Antibacterial performance of Ga-doped implants

Previous Ga-loaded Ti implants have shown excellent antibacterial efficacy against orthopaedic implant-related infections with *S. aureus* and *P. aeruginosa* [21]. The oral cavity comprises a diversity of microorganisms that *'race to invade'* the dental implant surface and compete with the host cells to establish contact [4]. In the current study, we have used a clinically relevant human oral saliva (polymicrobial) biofilm model to evaluate the antibacterial efficacy of modified implant surfaces. Live/dead staining of the substrates on days 1, 3, and 7 showed that Ga-doped surfaces, both Ti−Ga and TNP-Ga, had a significantly high percentage of dead cells compared to the undoped substrates (Fig. 6a). Quantification of the live/dead images showed that about 50% of the microbes present on the surface were dead in both Ti−Ga and TNP-Ga groups at different time points (Fig. 6c). On day 1, TNP-Ga showed a significantly higher antibacterial effect than Ti−Ga surfaces, which correlates with the higher IBR observed from TNP-Ga, while on days 3 and 7, Ti−Ga showed more efficacy. Despite the low amount of Ga ions released from Ti−Ga (<1 μg) on day 7, they showed antibacterial efficacy with about 50% of dead microbial load, suggesting that even low concentrations of Ga can elicit an antibacterial effect [34].

The mode of action of Ga^{3+} on microbial cells is similar to that observed in mammalian cells; they substitute Fe^{3+} and bind with proteins and ligands. Ga can cause microbial cell death by two primary mechanisms: (a) they displace Fe from significant proteins and enzymes in the microbial cell and thereby disrupt cellular mechanisms and cause DNA damage, and (b) the displaced Fe gets released into the microenvironment and produces oxidative radicals that can induce apoptosis [58] Quantifying the total biomass formed on the various surfaces via crystal violet staining showed no significant difference between the Ga-doped and undoped surfaces (Fig. 6d). Interestingly XTT assay showed that the amount of metabolically active biofilms on both Ti−Ga and TNP-Ga surfaces was significantly lower than other substrates at all time points (Fig. 6e). This might be attributed to the fact that while crystal violet stains the entire biofilm (cells + ECM), XTT is specific for viable

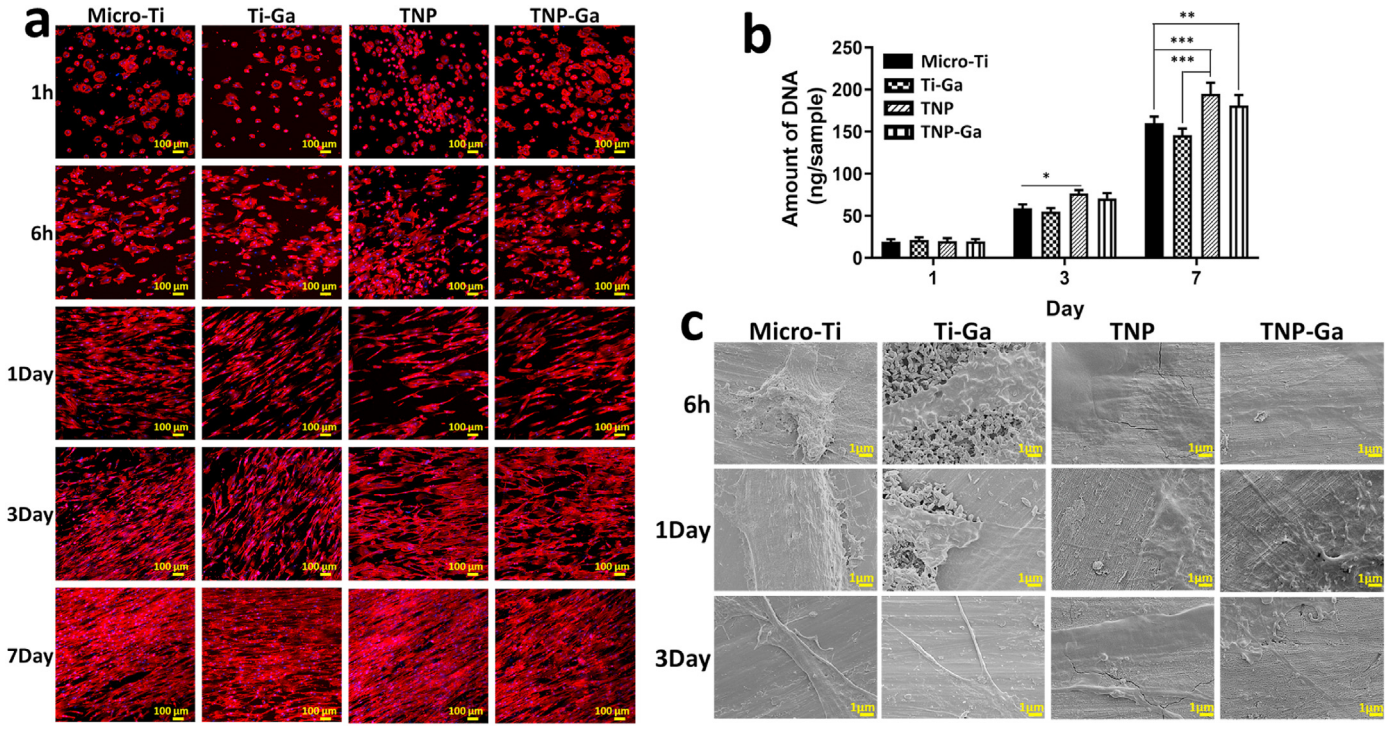

Fig. 5. Bioactivity of Ga doped Ti surfaces. (a) Actin-DAPI stained confocal images of hGF cells seeded on Micro, Ti−Ga, TNP, and TNP-Ga surfaces at 1 h, 6 h, days 1, 3, and 7. Red colour indicates actin filaments and blue indicates nuclei of cells. (b) Proliferation of hGFs on the Ti substrates on 1, 3 and 7 days. (c) Top-view SEM images of hGFs seeded on Micro, Ti−Ga, TNP and TNP-Ga surfaces at 6 h, days 1 and 3 showing filapodial extensions. *: Significant difference between the groups. (*-p<0.05, **-p<0.01, ***-p<0.001). hGF: human gingival fibroblasts. (For interpretation of the references to colour in this figure legend, the reader is referred to the Web version of this article.)

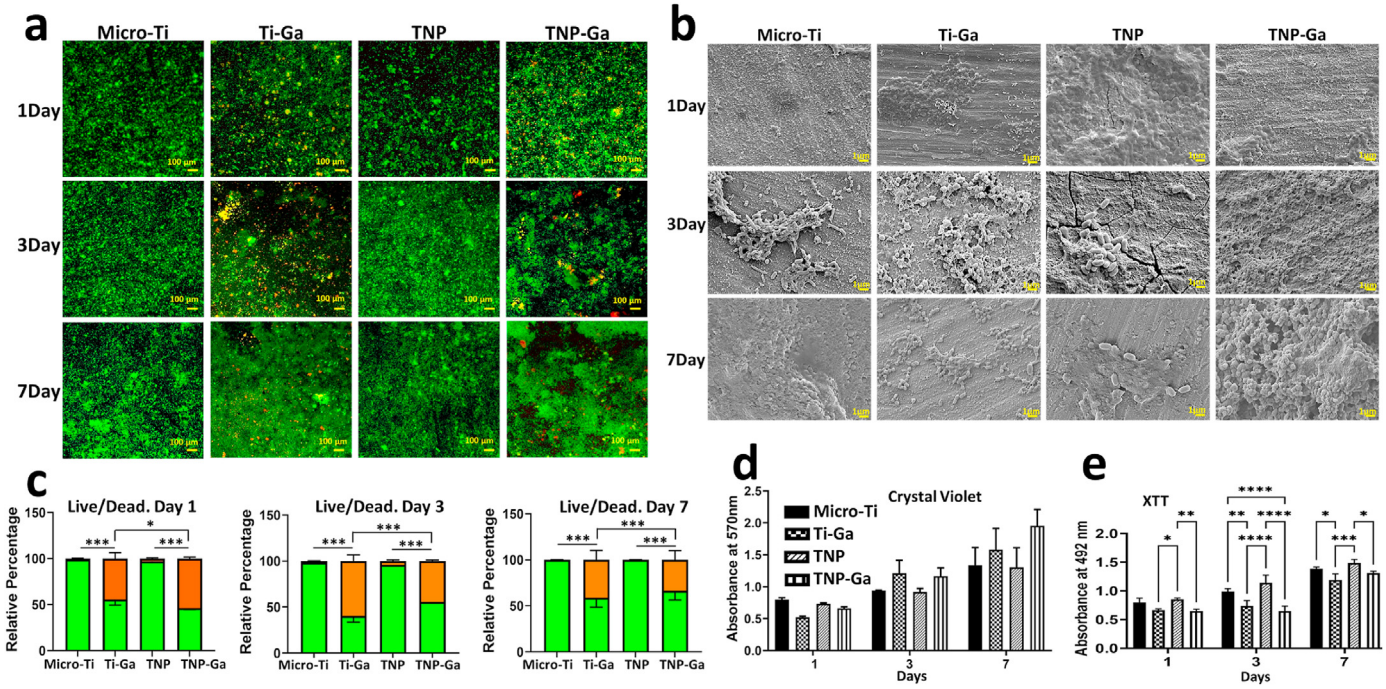

Fig. 6. Antibacterial efficacy against oral saliva biofilm model. (a) Live/Dead staining of biofilms on 1, 3 and 7 days by confocal imaging (green staining: biofilm, red staining: dead cells). (b) Morphology of biofilm formed on the Ti substrates on 1, 3 and 7 days captured via SEM. (c) Quantification of Live/Dead staining by *ImageJ*. (d) Quantification of total biofilm biomass by crystal violet staining. (e) Quantification of metabolically active biofilm by XTT assay. Ga-doped Ti showed a significantly high number of dead cells and biofilms with lower metabolic activity at all times. *: Significant difference between the groups. (*-$p<0.05$, **-$p<0.01$, ***-$p<0.001$). (For interpretation of the references to colour in this figure legend, the reader is referred to the Web version of this article.)

cells.

We performed SEM imaging to visualize biofilm attachment on modified Ti surfaces (Fig. 6b). At various time points, cocci and rod-shaped bacteria with intact cell morphology could be observed on Micro-Ti and TNP surfaces along with deposition of the extracellular matrix/ECM (extracellular polymeric substances). TNP-Ga surfaces showed high deposition of the ECM but a lower number of bacterial cells, which are consistent with the crystal violet and XTT results. The increased surface roughness of the TNP-Ga could stimulate excessive secretion of extracellular matrix in comparison to other groups [59].

The current study makes a pioneering attempt at evaluating the effect of Ga-doped titanium surfaces for dental implant applications. Ga ions were successfully doped on two surfaces, Micro-Ti (mimicking the micromachined dental implant surface) and TNPs (dual micro-nano structures with enhanced mechanical stability), followed by thorough physical/chemical characterizations. The doping of Ga was found to improve the surface roughness and wettability of the surfaces, which further helps modulate bioactivity. A sustained release of Ga ions was observed for 10 days from the surfaces and the released Ga ions did not show any toxicity toward human gingival fibroblasts. Further, TNPs were observed to modulate cellular attachment along the underlying micro-nanotopography. Finally, the antibacterial efficacy of Ga-doped surfaces against a clinically relevant polymicrobial oral saliva model was evaluated for the first time.

Despite the significant potential for the developed system to promote STI and inhibit biofilm formation, the current study has several limitations. While an overall antibacterial effect was observed, the impact that Ga has on various species present within the biofilm remains unexplored and experiments like next-generation sequencing need to be carried out to understand the detailed antimicrobial mechanism. Further, investigating the stability and therapeutic efficacy of the modified implant system in a physiologically relevant *in vivo* model is critical to ensure clinical translation. Despite a sustained release of Ga observed in the *in vitro* conditions, release kinetics and biodistribution of Ga in *in vivo* conditions may vary due to several factors like various enzymes, matrix metallo-proteases (MMPs) and the complex immune and circulatory systems present within the body. Radiolabelling the Ga ions and observing their release and biodistribution using an animal model would be an exciting avenue to explore in the future. Further, while reactive oxygen species (ROS) generation and ROS-induced apoptosis caused due to Ga concentrations in cancer cells like human leukemic cells have been studied previously [60,61], their effect on cells like osteoblasts, fibroblasts, and macrophages have not been adequately explored. In the current study, we did not observe any gingival fibroblast death or toxicity, however, this might be attributed to the low amount of Ga released. We recommend future studies focussed on investigating the influence of Ga release in a dose-dependent manner on the generation of ROS in osteoblasts and fibroblasts.

5. Conclusions

The transmucosal nature of dental implants and the ever-present pathogenic bacteria in the oral cavity presents a significant challenge to long-term implant success, especially in compromised patient conditions (aged, diabetic or smokers). To address this, various investigations have been carried out to modify the surface topography and chemistry of implants and facilitate bioactivity and therapeutic enhancements. Among the various surface modifications, electrochemically anodized Ti with titania nanopores (TNPs) have demonstrated outstanding potential in regulating soft-tissue integration (STI) and osseointegration. In the current study, we performed Ga doping of clinically relevant micro-

rough Ti and TNPs to achieve favorable implant bioactivity and antibacterial performances. The surface topography, chemistry and hydrophilicity of the TNPs and Ti surfaces were altered upon Ga-doping, resulting in the formation of Ga-containing nanoscale particulates that were firmly bound to the substrates. Further, the local release of Ga from the substrates did not cause any toxicity to the fibroblasts, and their favorable bioactivity on TNPs was maintained. Finally, the antibacterial efficacy of the Ga-doped substrates were demonstrated using a pertinent polymicrobial human oral salivary model (that mimics the physiological microflora of the oral cavity). Overall, Ga-doped nanoporous Ti implants show great potential in addressing the poor soft-tissue integration and bacterial infection challenges associated with conventional dental implants. This study paves the way for further optimizations of implant bioactivity and bactericidal performances based on chemically modified nano-engineered Ti implants. Future investigations on implant placement in long-term animal studies *in vivo* under mechanical loading are needed to bridge the gap between research and clinical translation.

Credit author statement

Anjana Jayasree: Conceptualization, Investigation, Methodology, Formal analysis, Writing – original draft, Visualization. Maria Natividad Gómez-Cerezo: Investigation, Formal analysis, Writing – review & editing. Elise Verron: Conceptualization, Methodology, Writing – review & editing. Sašo Ivanovski: Validation, Writing – review & editing, Supervision. Karan Gulati: Conceptualization, Methodology, Validation, Resources, Writing – review & editing, Supervision, Project administration, Funding acquisition.

Declaration of competing interest

The authors declare that they have no known competing financial interests or personal relationships that could have appeared to influence the work reported in this paper.

Acknowledgments

Anjana Jayasree is supported by the UQ Graduate School Scholarships (UQGSS), funded by the University of Queensland, Australia. Karan Gulati is supported by the National Health and Medical Research Council (NHMRC) Early Career Fellowship (APP1140699). This work was supported by the Australian Dental Research Foundation (ADRF) research grant. The authors acknowledge the facilities, and the scientific and technical assistance of the Australian Microscopy & Microanalysis Research Facility at the Centre for Microscopy and Microanalysis, The University of Queensland. This work was partly performed at the Queensland node of the Australian National Fabrication Facility. A company established under the National Collaborative Research Infrastructure Strategy to provide nano and microfabrication facilities for Australia's researchers. The authors would like to express our great appreciation to Professor Lisbeth Grondahl and Dr. Lachlan Casey for their generous help and assistance.

Appendix A. Supplementary data

Supplementary data to this article can be found online at https://doi.org/10.1016/j.mtadv.2022.100297.

References

[1] A. Jayasree, S. Ivanovski, K. Gulati, ON or OFF: Triggered therapies from anodized nano-engineered titanium implants, J. Contr. Release 333 (2021) 521–535, https://doi.org/10.1016/j.jconrel.2021.03.020.
[2] A. Besinis, S.D. Hadi, H.R. Le, C. Tredwin, R.D. Handy, Antibacterial activity and biofilm inhibition by surface modified titanium alloy medical implants following application of silver, titanium dioxide and hydroxyapatite nanocoatings, Nanotoxicology 11 (3) (2017) 327–338, https://doi.org/10.1080/17435390.2017.1299890.
[3] P.K. Moy, D. Medina, V. Shetty, T.L. Aghaloo, Dental implant failure rates and associated risk factors, Int. J. Oral Maxillofac. Implants 20 (4) (2005) 569–577.
[4] T. Guo, K. Gulati, H. Arora, P. Han, B. Fournier, S. Ivanovski, Race to invade: Understanding soft tissue integration at the transmucosal region of titanium dental implants, Dent, Mater. 37 (5) (2021) 816–831, https://doi.org/10.1016/j.dental.2021.02.005.
[5] T. Guo, K. Gulati, H. Arora, P. Han, B. Fournier, S. Ivanovski, Orchestrating soft tissue integration at the transmucosal region of titanium implants, Acta Biomater. 124 (2021) 33–49, https://doi.org/10.1016/j.actbio.2021.01.001.
[6] K. Gulati, M. Kogawa, S. Maher, G. Atkins, D. Findlay, D. Losic, Titania nanotubes for local drug delivery from implant surfaces, in: D. Losic, A. Santos (Eds.), Electrochemically Engineered Nanoporous Materials: Methods, Properties and Applications, Springer International Publishing, 2015, pp. 307–355. Cham.
[7] K. Gulati, H.-J. Moon, P.T.S. Kumar, P. Han, S. Ivanovski, Anodized anisotropic titanium surfaces for enhanced guidance of gingival fibroblasts, Mater. Sci. Eng. C 112 (2020) 110860, https://doi.org/10.1016/j.msec.2020.110860.
[8] A. Jayasree, N.T. Raveendran, T. Guo, S. Ivanovski, K. Gulati, Electrochemically nano-engineered titanium: Influence of dual micro-nanotopography of anisotropic nanopores on bioactivity and antimicrobial activity, Mater. Today Adv. 15 (2022) 100256, https://doi.org/10.1016/j.mtadv.2022.100256.
[9] D. Chopra, T. Guo, S. Ivanovski, K. Gulati, Single-step nano-engineering of multiple micro-rough metals via anodization, Nano Res (2022), https://doi.org/10.1007/s12274-022-4847-8.
[10] K. Gulati, H.-J. Moon, T. Li, P.T. Sudheesh Kumar, S. Ivanovski, Titania nanopores with dual micro-/nano-topography for selective cellular bioactivity, Mater. Sci. Eng. C 91 (2018) 624–630, https://doi.org/10.1016/j.msec.2018.05.075.
[11] K. Gulati, R.D.O. Martinez, M. Czerwiński, M. Michalska-Domańska, Understanding the influence of electrolyte aging in electrochemical anodization of titanium, Adv. Colloid Interface Sci. 302 (2022) 102615, https://doi.org/10.1016/j.cis.2022.102615.
[12] A. Al-Ahmad, M. Wiedmann-Al-Ahmad, A. Fackler, M. Follo, E. Hellwig, M. Bächle, C. Hannig, J.S. Han, M. Wolkewitz, R. Kohal, In vivo study of the initial bacterial adhesion on different implant materials, Arch. Oral Biol. 58 (9) (2013) 1139–11347, https://doi.org/10.1016/j.archoralbio.2013.04.011.
[13] R. Bürgers, T. Gerlach, S. Hahnel, F. Schwarz, G. Handel, M. Gosau, In vivo and in vitro biofilm formation on two different titanium implant surfaces, Clin. Oral Implants Res. 21 (2) (2010) 156–164, https://doi.org/10.1111/j.1600-0501.2009.01815.x.
[14] A. Mombelli, N.P. Lang, The diagnosis and treatment of peri-implantitis, Periodontology 17 (1) (2000) 63–76doi, https://doi.org/10.1111/j.1600-0757.1998.tb00124.x.
[15] J.A. Inzana, E.M. Schwarz, S.L. Kates, H.A. Awad, Biomaterials approaches to treating implant-associated osteomyelitis, Biomaterials 81 (2016) 58–71, https://doi.org/10.1016/j.biomaterials.2015.12.012.
[16] X. Li, B. Wu, H. Chen, K. Nan, Y. Jin, L. Sun, B. Wang, Recent developments in smart antibacterial surfaces to inhibit biofilm formation and bacterial infections, J. Mater. Chem. B 6 (26) (2018) 4274–4292, https://doi.org/10.1039/C8TB01245H.
[17] Y. Li, Y. Yang, l. Ruiyan, X. Tang, D. Guo, Y.A. Qing, Y. Qin, Enhanced antibacterial properties of orthopedic implants by titanium nanotube surface modification: a review of current techniques, Int. J. Nanomed. vol. Volume 14 (2019) 7217–7236, https://doi.org/10.2147/IJN.S216175.
[18] M.J.P. Biggs, R.G. Richards, N. Gadegaard, R.J. McMurray, S. Affrossman, C.D.W. Wilkinson, R.O.C. Oreffo, M.J. Dalby, Interactions with nanoscale topography: Adhesion quantification and signal transduction in cells of osteogenic and multipotent lineage, J. Biomed. Mater. Res., vol. 91A, no. 1 (2008), pp. 195-208 doi: 10.1002/jbm.a.32196.
[19] E. Zhang, X. Zhao, J. Hu, R. Wang, S. Fu, G. Qin, Antibacterial metals and alloys for potential biomedical implants, Bioact. Mater. 6 (8) (2021) 2569–2612, https://doi.org/10.1016/j.bioactmat.2021.01.030.
[20] X. Qu, H. Yang, B. Jia, M. Wang, B. Yue, Y. Zheng, K. Dai, Zinc alloy-based bone internal fixation screw with antibacterial and anti-osteolytic properties, Bioact. Mater. 6 (12) (2021) 4607–4624, https://doi.org/10.1016/j.bioactmat.2021.05.023.
[21] S. Maher, D. Linklater, H. Rastin, S.T.-Y. Liao, K. Martins de Sousa, L. Lima-Marques, P. Kingshott, H. Thissen, E.P. Ivanova, D. Losic, Advancing of 3D-printed titanium implants with combined antibacterial protection using ultrasharp nanostructured surface and gallium-releasing agents, ACS Biomater. Sci. Eng. 8 (1) (2021) 314–327, https://doi.org/10.1021/acsbiomaterials.1c01030.
[22] A. Cochis, B. Azzimonti, R. Chiesa, L. Rimondini, M. Gasik, Metallurgical gallium additions to titanium alloys demonstrate a strong time-increasing antibacterial activity without any cellular toxicity, ACS Biomater. Sci. Eng. 5 (6) (2019) 2815–2820, https://doi.org/10.1021/acsbiomaterials.9b00147.
[23] I. Strazic-Geljic, I. Guberovic, B. Didak, H. Schmid-Antomarchi, A. Schmid-Alliana, F. Boukhechba, J.-M. Bouler, J.-C. Scimeca, E. Verron, Gallium, a promising candidate to disrupt the vicious cycle driving osteolytic metastases,

Biochem. Pharmacol. 116 (2016) 11–21, https://doi.org/10.1016/j.bcp.2016.06.020.
[24] E. Verron, J.M. Bouler, J.C. Scimeca, Gallium as a potential candidate for treatment of osteoporosis, Drug Discov. Today 17 (19) (2012) 1127–1132, https://doi.org/10.1016/j.drudis.2012.06.007.
[25] E. Verron, M. Masson, S. Khoshniat, L. Duplomb, Y. Wittrant, M. Baud'huin, Z. Badran, B. Bujoli, P. Janvier, J.-C. Scimeca, J.-M. Bouler, J. Guicheux, Gallium modulates osteoclastic bone resorption in vitro without affecting osteoblasts, Br. J. Pharmacol. 159 (8) (2010) 1681–1692, https://doi.org/10.1111/j.1476-5381.2010.00665.x.
[26] N. Gómez-Cerezo, E. Verron, V. Montouillout, F. Fayon, P. Lagadec, J.M. Bouler, B. Bujoli, D. Arcos, M. Vallet-Regí, The response of pre-osteoblasts and osteoclasts to gallium containing mesoporous bioactive glasses, Acta Biomater. 76 (2018) 333–343, https://doi.org/10.1016/j.actbio.2018.06.036.
[27] I. Strazic Geljic, N. Melis, F. Boukhechba, S. Schaub, C. Mellier, P. Janvier, J.-P. Laugier, J.-M. Bouler, E. Verron, J.-C. Scimeca, Gallium enhances reconstructive properties of a calcium phosphate bone biomaterial, J. Tissue Eng. Regen. Med. 12 (2) (2017) e854–e866, https://doi.org/10.1002/term.2396.
[28] C. Mellier, F. Fayon, F. Boukhechba, E. Verron, M. LeFerrec, G. Montavon, J. Lesoeur, V. Schnitzler, D. Massiot, P. Janvier, O. Gauthier, J.-M. Bouler, B. Bujoli, Design and properties of novel gallium-doped injectable apatitic cements, Acta Biomater. 24 (2015) 322–332, https://doi.org/10.1016/j.actbio.2015.05.027.
[29] B.W. Stuart, G.E. Stan, A.C. Popa, M.J. Carrington, I. Zgura, M. Necsulescu, D.M. Grant, New solutions for combatting implant bacterial infection based on silver nano-dispersed and gallium incorporated phosphate bioactive glass sputtered films: A preliminary study, Bioact. Mater. 8 (2022) 325–340, https://doi.org/10.1016/j.bioactmat.2021.05.055.
[30] C. Zhang, B. Yang, J.M. Biazik, R.F. Webster, W. Xie, J. Tang, F.-M. Allioux, R. Abbasi, M. Mousavi, E.M. Goldys, K.A. Kilian, R. Chandrawati, D. Esrafilzadeh, K. Kalantar-Zadeh, Gallium nanodroplets are anti-inflammatory without interfering with Iron homeostasis, ACS Nano (2022), https://doi.org/10.1021/acsnano.1c10981.
[31] E. Verron, A. Loubat, G.F. Carle, C. Vignes-Colombeix, I. Strazic, J. Guicheux, N. Rochet, J.M. Bouler, J.C. Scimeca, Molecular effects of gallium on osteoclastic differentiation of mouse and human monocytes, Biochem. Pharmacol. 83 (5) (2012) 671–679, https://doi.org/10.1016/j.bcp.2011.12.015.
[32] S. Maher, D. Linklater, H. Rastin, P. Le Yap, E.P. Ivanova, D. Losic, Tailoring Additively Manufactured Titanium Implants for Short-Time Pediatric Implantations with Enhanced Bactericidal Activity, ChemMedChem 17 (2) (2021) e202100580, https://doi.org/10.1002/cmdc.202100580.
[33] J. Dong, D. Fang, L. Zhang, Q. Shan, Y. Huang, Gallium-doped titania nanotubes elicit anti-bacterial efficacy in vivo against Escherichia coli and Staphylococcus aureus biofilm, Materialia 5 (2019) 100209, https://doi.org/10.1016/j.mtla.2019.100209.
[34] H. Qiao, C. Zhang, X. Dang, H. Yang, Y. Wang, Y. Chen, L. Ma, S. Han, H. Lin, X. Zhang, J. Lan, Y. Huang, Gallium loading into a polydopamine-functionalised SrTiO3 nanotube with combined osteoinductive and antimicrobial activities, Ceram. Int. 45 (17, Part A) (2019) 22183–22195, https://doi.org/10.1016/j.ceramint.2019.07.240.
[35] T. Li, K. Gulati, N. Wang, Z. Zhang, S. Ivanovski, Bridging the gap: Optimized fabrication of robust titania nanostructures on complex implant geometries towards clinical translation, J. Colloid Interface Sci. 529 (2018) 452–463, https://doi.org/10.1016/j.jcis.2018.06.004.
[36] T. Guo, N.A.K. Oztug, P. Han, S. Ivanovski, K. Gulati, Old is gold: electrolyte aging influences the topography, chemistry, and bioactivity of anodized TiO2 nanopores, ACS Appl. Mater. Interfaces 13 (7) (2021) 7897–7912, https://doi.org/10.1021/acsami.0c19569.
[37] S. Ivanovski, H.R. Haase, P.M. Bartold, Isolation and characterization of fibroblasts derived from regenerating human periodontal defects, Arch. Oral Biol. 46 (8) (2001) 679–688, https://doi.org/10.1016/S0003-9969(01)00036-X.
[38] K. Gulati, T. Li, S. Ivanovski, Consume or conserve: microroughness of titanium implants toward fabrication of dual micro–nanotopography, ACS Biomater. Sci. Eng. 4 (9) (2018) 3125–3131, https://doi.org/10.1021/acsbiomaterials.8b00829.
[39] S. Suman, N. Mukurala, A.K. Kushwaha, Annealing induced surface restructuring in hydrothermally synthesized gallium oxide nano-cuboids, J. Cryst. Growth 554 (2021) 125946, https://doi.org/10.1016/j.jcrysgro.2020.125946.
[40] S. Yadav, K. Shrivas, P.K. Bajpai, Role of precursors in controlling the size, shape and morphology in the synthesis of copper sulfide nanoparticles and their application for fluorescence detection, J. Alloys Compd. 772 (2019) 579–592, https://doi.org/10.1016/j.jallcom.2018.08.132.
[41] T. Sultana, G.L. Georgiev, G. Auner, G. Newaz, H.J. Herfurth, R. Patwa, XPS analysis of laser transmission micro-joint between poly (vinylidene fluoride and titanium, Appl. Surf. Sci. 255 (5, Part 2) (2008) 2569–2573, https://doi.org/10.1016/j.apsusc.2008.07.149.
[42] D.A. Zatsepin, D.W. Boukhvalov, A.F. Zatsepin, Y.A. Kuznetsova, D. Gogova, V.Y. Shur, A.A. Esin, Atomic structure, electronic states, and optical properties of epitaxially grown β-Ga2O3 layers, Superlattice, Microst. 120 (2018) 90–100, https://doi.org/10.1016/j.spmi.2018.05.027.
[43] M. Suárez, A. Arias, J.R. Castillo-Saenz, M. Curiel-Alvarez, O. Pérez-Landeros, D. Mateos, E. Martínez-Guerra, A. Concha-Balderrama, B. Valdez-Salas, N. Nedev, Ultrahigh purity beta gallium oxide microstructures, Ceram. Int. (2022), https://doi.org/10.1016/j.ceramint.2022.05.205.
[44] C.-M. Han, H.-E. Kim, Y.-H. Koh, Creation of hierarchical micro/nano-porous TiO2 surface layer onto Ti implants for improved biocompatibility, Surf. Coating. Technol. 251 (2014) 226–231, https://doi.org/10.1016/j.surfcoat.2014.04.030.
[45] Y. Li, W. Wang, F. Yu, D. Wang, S. Guan, Y. Li, M. Qi, Characterization and cytocompatibility of hierarchical porous TiO2 coatings incorporated with calcium and strontium by one-step micro-arc oxidation, Mater Sci Eng C Mater Biol Appl 109 (2020) 110610, https://doi.org/10.1016/j.msec.2019.110610.
[46] M. Murphy, M.S. Walczak, A.G. Thomas, N. Silikas, S. Berner, R. Lindsay, Toward optimizing dental implant performance: Surface characterization of Ti and TiZr implant materials, Dent, Mater. 33 (1) (2017) 43–53doi, https://doi.org/10.1016/j.dental.2016.10.001.
[47] N.P. Lang, G.E. Salvi, G. Huynh-Ba, S. Ivanovski, N. Donos, D.D. Bosshardt, Early osseointegration to hydrophilic and hydrophobic implant surfaces in humans, Clin. Oral Implants Res. 22 (4) (2011) 349–356, https://doi.org/10.1111/j.1600-0501.2011.02172.x.
[48] Y. Yuan, M.P. Hays, P.R. Hardwidge, J. Kim, Surface characteristics influencing bacterial adhesion to polymeric substrates, RSC Adv. 7 (23) (2017) 14254–14261, https://doi.org/10.1039/C7RA01571B.
[49] R.N. Wenzel, Resistance of solid surfaces to wetting by water, Ind. Eng. Chem. 28 (8) (1936) 988–994, https://doi.org/10.1021/ie50320a024.
[50] V.S. Simi, N. Rajendran, Influence of tunable diameter on the electrochemical behavior and antibacterial activity of titania nanotube arrays for biomedical applications, Mater. Char. 129 (2017) 67–79, https://doi.org/10.1016/j.matchar.2017.04.019.
[51] H.-A. Pan, J.-Y. Liang, Y.-C. Hung, C.-H. Lee, J.-C. Chiou, G.S. Huang, The spatial and temporal control of cell migration by nanoporous surfaces through the regulation of ERK and integrins in fibroblasts, Biomaterials 34 (4) (2013) 841–853, https://doi.org/10.1016/j.biomaterials.2012.09.078.
[52] B. Santos Gomes, D.J. Morgan, W. Langbein, P. Borri, F. Masia, Biofunctionalisation of gallium arsenide with neutravidin, J. Colloid Interface Sci., vol. 608 (2022), pp. 2399-2406 doi: 10.1016/j.jcis.2021.10.135.
[53] J.C. Scimeca, E. Verron, Nano-engineered biomaterials: Safety matters and toxicity evaluation, Mater. Today Adv. 15 (2022), 100260, https://doi.org/10.1016/j.mtadv.2022.100260.
[54] K. Gulati, J.-C. Scimeca, S. Ivanovski, E. Verron, Double-edged sword: Therapeutic efficacy versus toxicity evaluations of doped titanium implants, Drug Discov. Today 26 (11) (2021) 2734–2742, https://doi.org/10.1016/j.drudis.2021.07.004.
[55] A. Milheiro, K. Nozaki, C.J. Kleverlaan, J. Muris, H. Miura, A.J. Feilzer, In vitro cytotoxicity of metallic ions released from dental alloys, Odontology 104 (2) (2016) 136–142, https://doi.org/10.1007/s10266-014-0192-z.
[56] L.R. Bernstein, Mechanisms of therapeutic activity for gallium, Pharmacol. Rev. 50 (4) (1988) 665. http://pharmrev.aspetjournals.org/content/50/4/665.abstract [Online]. Available:.
[57] L.E. McNamara, T. Sjöström, K. Seunarine, R.M.D. Meek, B. Su, M.J. Dalby, Investigation of the limits of nanoscale filopodial interactions, J. Tissue Eng. 5 (2018), 2041731414536177, https://doi.org/10.1177/2041731414536177.
[58] Z. Xu, X. Zhao, X. Chen, Z. Chen, Z. Xia, Antimicrobial effect of gallium nitrate against bacteria encountered in burn wound infections, RSC Adv. 7 (2017) 52266–52273, https://doi.org/10.1039/C7RA10265H.
[59] A.V. Singh, V. Vyas, R. Patil, V. Sharma, P.E. Scopelliti, G. Bongiorno, A. Podestà, C. Lenardi, W.N. Gade, P. Milani, Quantitative characterization of the influence of the nanoscale morphology of nanostructured surfaces on bacterial adhesion and biofilm formation, PLoS One 6 (9) (2011) e25029, https://doi.org/10.1371/journal.pone.0025029.
[60] C.R. Chitambar, Medical applications and toxicities of gallium compounds, Int. J. Environ. Res. Publ. Health 7 (5) (2010) 2337–2361 [Online]. Available: https://www.mdpi.com/1660-4601/7/5/2337.
[61] M. Yang, S.H. Kroft, C.R. Chitambar, Gene expression analysis of gallium-resistant and gallium-sensitive lymphoma cells reveals a role for metal-responsive transcription factor-1, metallothionein-2A, and zinc transporter-1 in modulating the antineoplastic activity of gallium nitrate, Mol. Cancer Therapeut. 6 (2) (2007) 633–643, https://doi.org/10.1158/1535-7163.MCT-06-0557.